6. S. E. Gustafsson, N. O. Halling and R. A. E. Kjellander, Optical determination of thermal conductivity with a plane source technique, *Z. Naturforsch* **23a,** H.1, 44–47 (1968); *Z. Naturforsch* **23a,** H.5, 682–686 (1968).
7. O. Odawara, I. Okada and K. Kawamura, Measurement of thermal diffusivity of HTS by optical interferometry, *J. Chem. Engng Data* **22**(2), 222–225 (1977).
8. Y. Iwadate, I. Okada and K. Kawamura, Thermal conductivity of molten KNO_3–$NaNO_2$ mixtures measured with wave-front shearing interferometry, *J. Chem. Soc. Japan, Chem. Ind. Chem.* **6,** 969–976 (1982).
9. G. Sibois, Thèse de Spécialité, Université de Provence, France (1980).
10. W. E. Kirst, W. M. Nagle and J. B. Castner, A new heat transfer medium for high temperature, *Trans. Am. Inst. Chem. Engrs* **36,** 371–394 (1940).
11. P. W. Bridgman, *The Physics of High Pressures.* G. Bell & Sons, London (1949).
12. H. Bloom, A. Doroszkowski and S. B. Tricklebank, Molten salts mixtures. IX*. The thermal conductivities of molten nitrate systems, *Aust. J. Chem.* **18,** 1171–1176 (1965).
13. J. McDonald, Ph.D. thesis, University of Minnesota (1969).
14. E. McLaughlin, *Theory of Thermal Conductivity of Fluids, Thermal Conductivity* (edited by R. P. Tye), Vol. 2, pp. 1–64. Academic Press, New York (1969).
15. A. G. Turnbull, The thermal conductivity of molten salts. A transient measurement method, *Aust. J. Appl. Sci.* **12,** 30–41 (1960).
16. M. Berthet and J. J. Peninou, Stockage thermique sous forme de chaleur latente à basse température, Colloque DGRST, Sophia Antipolis, October (1978).
17. W. D. Powers, Thermal properties of molten salts, A.N.P. Quarterly Progress Report, Report ONRL, 30 September, OTS-U.S. Dept. of Commerce (1957).
18. H. W. Hoffman, Physical properties and heat transfer characteristics of alkali nitrate–nitrite salt mixture, Report ONRL, 21 July, OTS-U.S. Dept. of Commerce (1955).

Int. J. Heat Mass Transfer. Vol. 27, No. 4, pp. 626–630, 1984
Printed in Great Britain

0017-9310/84 $3.00 + 0.00

A STUDY OF THE VARIATION OF THE PRESSURE IN A NATURAL CIRCULATION LOOP

A. MERTOL,† A. LAVINE and R. GREIF
Department of Mechanical Engineering, University of California, Berkeley, CA 94720, U.S.A.

(*Received* 27 *August* 1982 *and in revised form* 4 *May* 1983)

NOMENCLATURE

c	specific heat
D	dimensionless parameter, $2\pi Rh/crV\rho_w$
f	friction coefficient, $2\tau_w/\rho_w v^2$
g	acceleration of gravity
h	heat transfer coefficient per unit of length
p	dimensionless pressure
Δp	pressure difference, $p(\theta,\tau)-p(0,\tau)$
p_t	dimensionless total pressure, $2p_t^*/\rho_w V^2$
p_t^*	total pressure
q	heat flux, cf. Fig. 1
R	radius of the circular loop, cf. Fig. 1
Re	Reynolds number, $\rho_w v 2r/\mu$
r	radius of the toroid, cf. Fig. 1
T	temperature
T_w	constant wall temperature for the upper loop, cf. Fig. 1
t	time
V	characteristic velocity, $(g\beta Rrq/2\pi c\mu)^{1/2}$
v	velocity of the fluid
w	dimensionless velocity, v/V.

Greek symbols

β	thermal expansion coefficient
Γ	dimensionless parameter, $16\pi\mu R/\rho_w r^2 V$
θ	space coordinate, cf. Fig. 1
μ	absolute viscosity
ρ_w	reference density evaluated at the wall temperature, T_w
ϕ	dimensionless temperature, $h(T-T_w)/q$
τ	dimensionless time, $Vt/2\pi R$
τ_w	shear stress, $f\rho_w v^2/2$.

Subscripts

avg	average over the loop
d	dynamic
s	static
ss	steady state.

INTRODUCTION

A STUDY has been made of the steady-state and transient pressure variation in a closed toroidal natural convection loop (cf. Fig. 1). The loop is heated over the lower half and cooled over the upper half. The resulting density variation causes the fluid to flow. Previous studies of toroidal loops have presented the temperature distributions, flow rates and stability characteristics [1–9]. A number of related studies have also been carried out [10–16]. The present work differs from previous studies in that the pressure distribution is now presented. Limiting analytical expressions have also been derived for the steady-state pressure distributions. To aid in the understanding of the results, the temperature distributions have also been presented along with the limiting expressions [3].

ANALYSIS

The toroidal loop is heated with a constant flux, q, over the lower half, $\pi < \theta < 2\pi$, and cooled by maintaining a constant wall temperature, T_w, over the upper half, $0 < \theta < \pi$. The flow is assumed to be laminar and in the counter-clockwise direction. The dimensionless forms of the momentum and energy equations are [1–3]:

$$\frac{\partial p_t}{\partial \theta} = -\frac{1}{\pi}\frac{\mathrm{d}w}{\mathrm{d}\tau} - \frac{2gR}{V^2}\cos\theta + \frac{\pi}{2}\frac{\Gamma}{D}\phi\cos\theta - \frac{\Gamma}{\pi}w, \quad (1)$$

and

$$\frac{\partial \phi}{\partial \tau} + 2\pi w\frac{\partial \phi}{\partial \theta} = \begin{cases} -2D\phi, & 0 < \theta < \pi, \quad (2a) \\ 2D, & \pi < \theta < 2\pi. \quad (2b) \end{cases}$$

† Present address: Passive Research and Development Group, Lawrence Berkeley Laboratory, University of California, Berkeley, CA 94720, U.S.A.

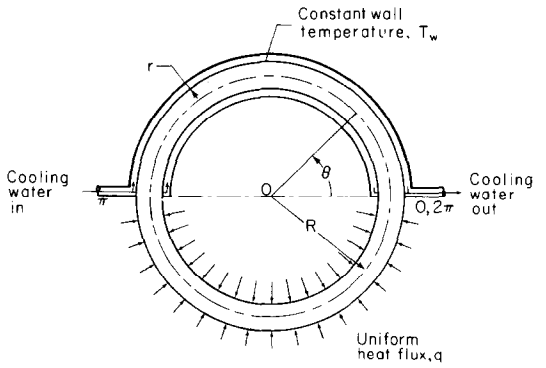

FIG. 1. The circular, toroidal natural circulation loop.

The temperature distributions have been obtained previously [3]. Using these results, the pressure may now be obtained by integrating equation (1):

$$\Delta p_d(\theta,\tau) = p_d(\theta,\tau) - p_d(0,\tau) = -\left(\frac{dw}{d\tau} + \Gamma w\right)\frac{\theta}{\pi} + \frac{\pi\Gamma}{2D}\int_0^\theta (\phi - \phi_{avg})\cos\theta\, d\theta, \quad (3)$$

where

$$p_d = p_t - p_s, \quad (4a)$$

and

$$p_s = \frac{p_s^*}{\rho_w V^2/2} = -\frac{\rho_{avg} gR\sin\theta}{\rho_w V^2/2} = -\frac{2gR\sin\theta}{V^2}\frac{\rho_{avg}}{\rho_w}. \quad (4b)$$

Steady-state pressure distributions may be obtained from equation (3) by setting $dw/d\tau = 0$ and using the steady-state profiles of [3]:

$$\Delta p_{d_{ss}}(\theta) = \begin{cases} \dfrac{\Gamma}{2w_{ss}}\dfrac{e^{-D\theta/\pi w_{ss}}\left(\pi\sin\theta - \dfrac{D}{w_{ss}}\cos\theta\right) + D/w_{ss}}{(1-e^{-D/w_{ss}})[1+(D/\pi w_{ss})^2]} - \Gamma\dfrac{\theta}{\pi}w_{ss} - \dfrac{\pi}{2}\dfrac{\Gamma}{D}\phi_{avg_{ss}}\sin\theta, & 0 \le \theta \le \pi, \quad (5a) \\ \dfrac{\Gamma}{2w_{ss}}\left[\theta\sin\theta + \cos\theta - 1 + \pi\sin\theta\left(\dfrac{2e^{-D/w_{ss}}-1}{1-e^{-D/w_{ss}}}\right)\right] - \Gamma\left(\dfrac{\theta}{\pi} - 2\right)w_{ss} - \dfrac{\pi}{2}\dfrac{\Gamma}{D}\phi_{avg_{ss}}\sin\theta, & \pi \le \theta \le 2\pi, \quad (5b) \end{cases}$$

where

$$\phi_{avg_{ss}} = \frac{1}{2} + \frac{D}{2w_{ss}}\left(\frac{1}{2} + \frac{e^{-D/w_{ss}}}{1-e^{-D/w_{ss}}}\right). \quad (5c)$$

Note that the continuity of pressure at $\theta = 0, 2\pi$ and $\theta = \pi^+, \pi^-$ was used.†

Limiting expressions for the pressure may be obtained. For large values of D, $w_{ss} \approx 1/\sqrt{2}$ and $\phi_{avg_{ss}} \approx \sqrt{(2)}D/4$ [3], which then yields

$$\frac{\Delta p_{d_{ss}}(\theta)}{\Gamma} = \begin{cases} -\dfrac{1}{\sqrt{2}}\left(\dfrac{\theta}{\pi} + \dfrac{\pi}{4}\sin\theta\right), & 0 \le \theta \le \pi, \quad (6a) \\ \dfrac{1}{\sqrt{2}}\left[(\theta - 5\pi/4)\sin\theta + \cos\theta + \left(1 - \dfrac{\theta}{\pi}\right)\right], & \pi \le \theta \le 2\pi. \quad (6b) \end{cases}$$

For small values of D, $w_{ss} \approx 1$ and $\phi_{avg_{ss}} \approx 1$ [3], and

$$\frac{\Delta p_{d_{ss}}(\theta)}{\Gamma} = \begin{cases} \dfrac{1}{2}\left[\left(\dfrac{\pi}{2} - \theta\right)\sin\theta - \cos\theta + 1\right] - \dfrac{\theta}{\pi}, & 0 \le \theta \le \pi, \quad (7a) \\ \dfrac{1}{2}\left[\left(\theta - 3\dfrac{\pi}{2}\right)\sin\theta + \cos\theta - 1\right] - \left(\dfrac{\theta}{\pi} - 2\right), & \pi \le \theta \le 2\pi. \quad (7b) \end{cases}$$

† The pressure, $p_{d_{ss}}(\theta)$, is continuous at $\theta = 0$ and at $\theta = \pi$. For the $\theta = \pi$ case, the equality of the pressure [cf. equations (5a) and (5b)] is readily obtained when equation (11) of ref. [3] is used.

The location of the extrema are obtained by differentiating equation (5) and setting the result to zero. For the upper loop we obtain

$$\frac{1}{\Gamma}\frac{dp_{d_{ss}}(\theta)}{d\theta} = \frac{\pi}{2w_{ss}}\left[\frac{e^{-D\theta/\pi w_{ss}}\cos\theta}{1-e^{-D/w_{ss}}}\right] - \frac{w_{ss}}{\pi} - \frac{\pi}{2D}\phi_{avg_{ss}}\cos\theta = 0, \quad 0 \le \theta \le \pi, \quad (8a)$$

and for the lower loop

$$\frac{1}{\Gamma}\frac{dp_{d_{ss}}(\theta)}{d\theta} = \frac{1}{2w_{ss}}\left[\theta + \pi\left(\frac{2e^{-D/w_{ss}}-1}{1-e^{-D/w_{ss}}}\right)\right]\cos\theta - \frac{w_{ss}}{\pi} - \frac{\pi}{2D}\phi_{avg_{ss}}\cos\theta = 0, \quad \pi \le \theta \le 2\pi. \quad (8b)$$

For small and large values of D the above equations may be simplified.

For completeness, limiting expressions are presented for the steady-state temperature distributions. For small values of D one obtains (cf. equation (10) of ref. [3])

$$\phi_{ss}(\theta) = \begin{cases} 1 - D\dfrac{\theta}{\pi}, & 0 \le \theta \le \pi, \quad (9a) \\ 1 + D\dfrac{\theta}{\pi}, & \pi \le \theta \le 2\pi. \quad (9b) \end{cases}$$

For large values of D, the relations are:

$$\phi_{ss}(\theta) = \begin{cases} 0, & 0^+ \le \theta \le \pi, \quad (10a) \\ \sqrt{(2)}D\left(\dfrac{\theta}{\pi} - 1\right), & \pi \le \theta \le 2\pi^-. \quad (10b) \end{cases}$$

Note that for large values of D, the temperature is not continuous at $\theta = 0, 2\pi$.

RESULTS AND DISCUSSION

The steady-state temperature distribution, $\phi_{ss}(\theta)$, will be referred to below and is therefore presented in Fig. 2 which is obtained from ref. [3]. The constant heat input yields a linear increase in the temperature over $\pi \le \theta \le 2\pi$. In the cooling section the heat loss is proportional to the difference in the temperature between the fluid and the wall which yields an exponential decrease in the temperature as a function of θ.

For small and large values of D, equation (11) of ref. [3] yields $w_{ss} \approx 1$ and $1/\sqrt{2}$, respectively. From the definitions of w

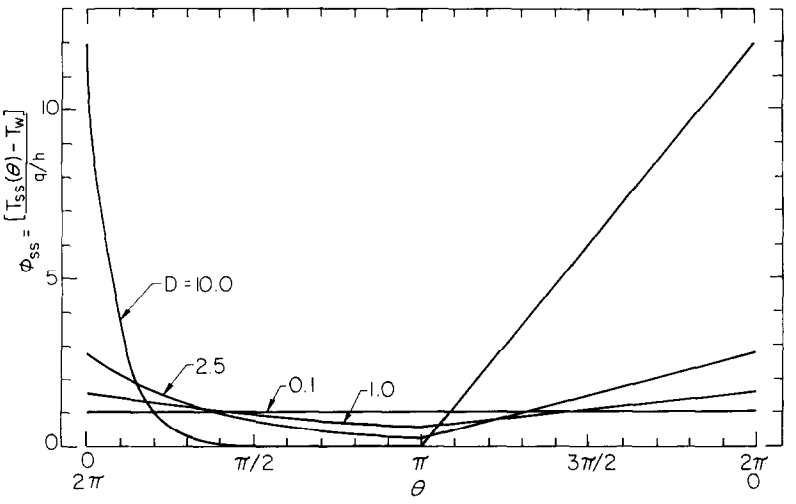

FIG. 2. Steady-state temperature distribution.

and V it then follows that $v_{ss} \sim q^{1/2}$ for both cases. An energy balance over the heating section under steady-state conditions yields

$$q = \left(\frac{\rho c r}{2\pi R}\right) v_{ss}[T_{ss}(0) - T_{ss}(\pi)]. \tag{11}$$

Using the limiting result $v_{ss} \sim q^{1/2}$ and equation (11) yields, for either small or large D:

$$T_{ss}(0) - T_{ss}(\pi) \sim q^{1/2}, \tag{12a}$$

or

$$\phi_{ss}(0) - \phi_{ss}(\pi) \sim q^{-1/2}. \tag{12b}$$

For small D (large heat flux, q) the temperature difference between the exit ($\theta = 0$) and the inlet ($\theta = \pi$) to the heating section is large. Note that the corresponding dimensionless values are small (cf. Fig. 2). However, for large D (small q) the temperature difference is now small while the dimensionless temperature difference is large.

An energy balance over the cooling section for steady-state conditions yields

$$q = \frac{h}{\pi} \int_0^{\pi} [T_{ss}(\theta) - T_w] \, d\theta, \tag{13a}$$

or

$$1 = \frac{1}{\pi} \int_0^{\pi} \phi_{ss}(\theta) \, d\theta = \phi_{avg_{ss}}(\text{cooling section}). \tag{13b}$$

The dimensional form of equation (13) is

$$T_{avg_{ss}} - T_w = \frac{q}{h}. \tag{14}$$

For small D (large q and/or small h) the average temperature of the cooling section is much greater than the wall temperature, T_w, while for increasing values of D these two temperatures approach one another.

The average temperature of the heating section is attained at the location $\theta = 3\pi/2$. The *average temperature of the loop* is the mean of the average temperatures of the heating and cooling sections. Therefore the fluid reaches the value of the average loop temperature in both the heating and cooling sections. The system parameter D determines these locations. For small values of D, the locations are close to the centers of the heating and cooling sections; that is, close to $\theta = 3\pi/2$ and $\theta = \pi/2$, respectively. For increasing values of D, they move away from the centers; in the heating section towards the heating inlet and in the cooling section towards the cooling inlet (cf. Fig. 2). The regions where the values of the average loop temperature are attained are given by $5\pi/4 \leqslant \theta \leqslant 3\pi/2$ and $0 \leqslant \theta \leqslant \pi/2$.

For the (dimensionless) pressure, we see that a pressure, p_s, has been subtracted from the total pressure, p_t [equation (4a)]. The pressure, p_s, is the hydrostatic pressure only when the temperature in the loop is *everywhere* equal to the average temperature of the loop, T_{avg}. Therefore, the pressure p_d is a reasonable approximation to the dynamic pressure. From equation (3) we see that under steady-state conditions ($dw/d\tau = 0$) the change in the dynamic pressure is balanced by buoyancy (relative to the average density) and friction. The datum for the pressure has been taken to be the value at $\theta = 0$. Friction always opposes the flow, contributing to a negative pressure gradient, while buoyancy acts to assist the flow at some locations and oppose the flow in others. Hence the pressure gradient is positive when buoyancy assists the flow strongly enough to overcome the friction.

The steady-state and the transient dynamic pressure are given in Figs. 3(a) and (b), respectively. In Fig. 3(a), for small D, the hot fluid emerging from the heated section enters the cooling section at $\theta = 0$ with a lower than average density (buoyant) and overcomes the friction force; as a result the pressure is increasing. However, as the fluid moves through the cooling section, it becomes cooler (less buoyant) and the pressure levels off. The frictional force then becomes more important and the pressure starts to decrease. After the fluid passes $\theta = \pi/2$ (where it reached the average loop temperature for the case as $D \to 0$) its greater than average density contributes to driving the flow and begins to overwhelm the friction. Thus the pressure increases again (at $\theta \approx 3\pi/4$). After entering the heating section ($\theta = \pi$), the fluid becomes less dense and buoyancy is less effective in driving the flow. Therefore the pressure levels off and then decreases. After $\theta = 3\pi/2$, the lighter fluid once again drives the flow and the pressure increases at $\theta \approx 7\pi/4$.†

For large D, the fluid cools very rapidly in the cooling region and becomes denser than average. Thus the pressure rapidly decreases as both gravity and friction oppose the flow. After $\theta = \pi/2$ the dense fluid assists the flow in the loop and the

† Note that for small D, the region $\pi/2 \leqslant \theta \leqslant 3\pi/2$ is anti-buoyant, and the regions $0 \leqslant \theta \leqslant \pi/2$ and $3\pi/2 \leqslant \theta \leqslant 2\pi$ are buoyant. A detailed discussion of the buoyant and anti-buoyant regions is given in ref. [7].

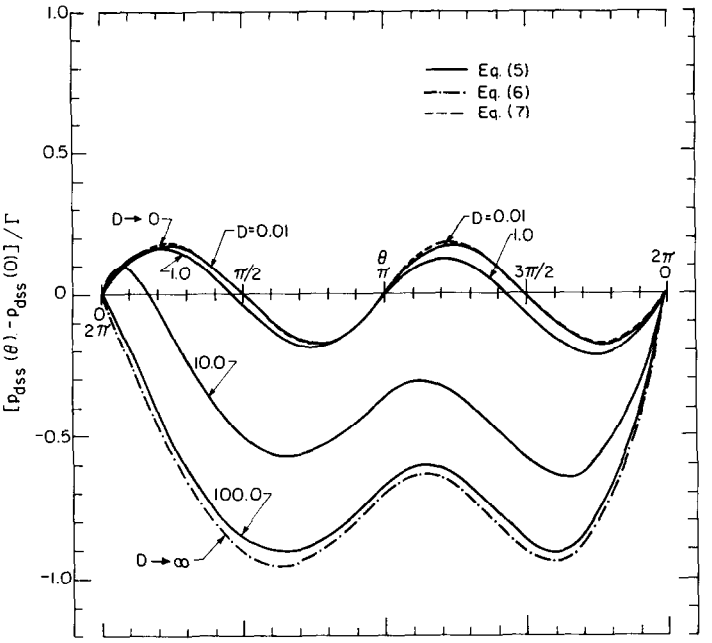

FIG. 3(a). Steady-state pressure distribution.

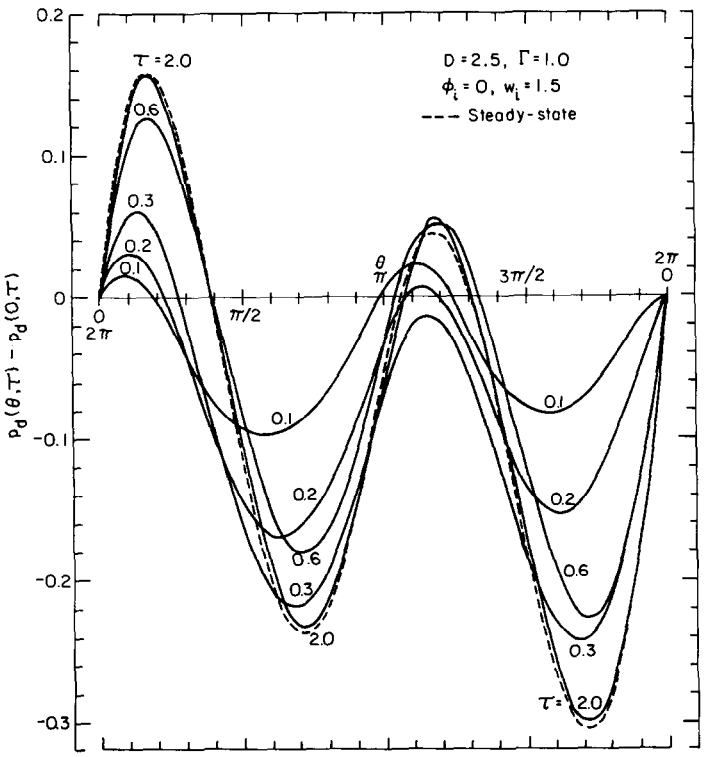

FIG. 3(b). Transient pressure distribution.

pressure increases. After entering the heating section the fluid becomes less dense and the behavior in this region is similar to that given for small D.

For the transient study, calculations were begun at time $\tau = 0$, for a specified velocity, w_i, in the counter-clockwise direction and a temperature, ϕ_i. The finite-difference method of ref. [3] was used. The temperature and the velocity were solved simultaneously from the integrated form of equation (1) around the loop and from equation (2). The resulting values were then substituted into equation (3) to obtain the pressure. Typical results are given in Fig. 3(b).

For small time, the hot fluid leaving the heating section has only moved a small distance in the cooling section. Therefore, it is only within a small 'penetration depth' near $\theta = 0^+$ that heating assists the flow *in the cooling section.* Beyond this region $\phi = \text{const.} = \phi_i = 0$ in the cooling section and the pressure decreases until $\theta \approx \pi/2$. Beyond $\theta \approx \pi/2$ the flow is aided by gravity. In the heating section the cold fluid has only penetrated to a region near $\theta = \pi^+$ and in this region the flow is aided. Outside this region, $\phi = \text{const.}$ and the flow is opposed up to $\theta \approx 3\pi/2$ and aided over $3\pi/2 < \theta < 2\pi$.

While the variation of the dynamic pressure is of interest, the ratio of the maximum dynamic pressure to the maximum hydrostatic pressure is of greater significance, namely

$$\left|\frac{\Delta p_{d_{max}}}{\Delta p_{s_{max}}}\right| \simeq \frac{\Gamma \rho_w V^2/2}{\rho_w g R} = 10.0\left(\frac{\beta R q \mu}{\rho_w^2 g r^3 c}\right)^{1/2} = 4.5 \times 10^{-6} q^{1/2}. \quad (15)$$

For the experimental system of refs. [1, 2], $R = 0.38$ m, $r = 0.015$ m, and q varies from 1000 to 4000 W m^{-2} for stable runs [6]. Water properties are evaluated at $T = 27$°C. Thus, the static pressure is up to four orders of magnitude greater than the dynamic pressure. Therefore, the total pressure is essentially hydrostatic.

Acknowledgements—The authors are grateful to the National Science Foundation for support, under Grant No. MEA 81-07202 and to Mr A. Giz for his helpful comments.

REFERENCES

1. H. F. Creveling, J. F. de Paz, J. Y. Baladi and R. J. Schoenhals, Stability characteristics of a single-phase free convection loop, *J. Fluid Mech.* **67,** 65–84 (1975).
2. P. S. Damerell and R. J. Schoenhals, Flow in a toroidal thermosyphon with angular displacement of heated and cooled sections, *J. Heat Transfer* **101,** 672–676 (1979).
3. R. Greif, Y. Zvirin and A. Mertol, The transient and stability behavior of a natural convection loop, *J. Heat Transfer* **101,** 684–688 (1979).
4. Y. Zvirin, The effect of dissipation on free convection loops, *Int. J. Heat Mass Transfer* **22,** 1539–1546 (1979).
5. A. Mertol, R. Greif and Y. Zvirin, The transient, steady state and stability behavior of a thermosyphon with throughflow, *Int. J. Heat Mass Transfer* **24,** 621–633 (1981).
6. A. Mertol, R. Greif and Y. Zvirin, Two dimensional study of heat transfer and fluid flow in a natural convection loop, *J. Heat Transfer* **104,** 508–514 (1982).
7. A. Mertol and R. Greif, Study of a thermosyphon with a counter-flow heat exchanger, in *Proc. 7th Int. Heat Transfer Conf.*, Vol. 2, pp. 239–244. Munich, Fed. Rep. of Germany (1982).
8. A. Mertol, R. Greif and A. T. Giz, The transient, steady-state and stability behavior of a toroidal thermosyphon with a parallel-flow heat exchanger, *ASME J. Solar Energy Engng* **105,** 58–65 (1983).
9. E. Wacholder, S. Kaizerman and E. Elias, Numerical analysis of the stability and transient behavior of natural convection loops, *Int. J. Engng. Sci.* **20,** 1235–1254 (1982).
10. B. J. Huang, Similarity theory of solar water heater with natural circulation, *Solar Energy* **25,** 105–116 (1980).
11. H. H. Bau and K. E. Torrance, Transient and steady behavior of an open, symmetrically-heated, free convection loop, *Int. J. Heat Mass Transfer* **24,** 597–609 (1981).
12. H. H. Bau and K. E. Torrance, On the stability and flow reversal of an asymmetrically heated open convection loop, *J. Fluid Mech.* **106,** 417–433 (1981).
13. Y. Zvirin, P. R. Jeuck, C. W. Sullivan and R. B. Duffey, Experimental and analytical investigation of a natural circulation system with parallel loops, *J. Heat Transfer* **103,** 645–652 (1981).
14. Y. Zvirin, A review of natural circulation loops in pressurized water reactors and other systems, *Nucl. Engng Design* **67,** 203–225 (1981).
15. A. Mertol, W. Place, T. Webster and R. Greif, Detailed loop model (DLM) analysis of liquid solar thermosyphons with heat exchangers, *Solar Energy* **27,** 367–386 (1981).
16. K. Chen, The influence of loop configuration on closed-loop thermosyphons, ASME Paper No. 82-WA/HT-63.

Int. J. Heat Mass Transfer. Vol. 27, No. 4, pp. 630 633, 1984
Printed in Great Britain

0017 9310/84 $3.00 + 0.00

HIGH RAYLEIGH NUMBER HEAT TRANSFER IN A HORIZONTAL CYLINDER WITH ADIABATIC WALL

G. H. SCHIROKY* and F. ROSENBERGER

Departments of Physics, and Materials Science and Engineering, University of Utah, Salt Lake City, UT 84112, U.S.A.

(*Received* 29 *September* 1982 *and in revised form* 11 *July* 1983)

NOMENCLATURE

A	cross-sectional area of cylinder [m^2]
C	Gill's free constant, dimensionless
d'	dimensionless width of thermal boundary layer, l/m
d	width of thermal boundary layer, $d'L$ [m]
g	gravitational acceleration [m s^{-2}]
h	height of rectangular enclosure [m]
k	fluid thermal conductivity [W m^{-1} K^{-1}]
k_1	dimensionless axial temperature gradient in cylinder core region
L	length of cylinder, or width of rectangular 2-D enclosure [m]
m	constant, dimensionless, equation (2)

* Present address: GA Technologies, P.O. Box 81608, San Diego, CA 92138, U.S.A.